Spatial distribution of charge-density-wave phase slip in $NbSe_3$

S. G. Lemay, M. C. de Lind van Wijngaarden, T. L. Adelman, and R. E. Thorne
Laboratory of Atomic and Solid State Physics, Clark Hall, Cornell University, Ithaca, New York 14853-2501
(Received 24 November 1997)

Steady-state charge transport via motion of charge-density waves (CDW's) requires conversion between collective CDW conduction and quasiparticle conduction in the vicinity of current injection contacts. The conversion occurs via phase slip, in which CDW amplitude defects form and move in the presence of CDW strain so as to remove or add CDW phase fronts in a process analogous to phase slip in superconductors and superfluids. We have determined the spatial distribution of phase slip for the T_{P_1} CDW in $NbSe_3$ by measuring the spatial variation of the CDW current density $j_c(x)$. As the current contacts are approached, $j_c(x)$ decreases and the normal current $j_n(x)$ due to quasiparticle flow increases. The size of the region near each contact where appreciable phase slip occurs is less than 40 μm for T near 120 K but grows to hundreds of micrometers at lower temperatures. The current and phase-slip profiles are asymmetric with respect to driving current direction, implying an asymmetry between phase front addition and removal. Analysis of these profiles yields the local relation between the phase-slip rate $r_{ps}(x)$ and CDW strain $\epsilon(x)$. This relation is not unique, and for a given strain the phase-slip rate increases with increasing distance from the current electrode. These results are inconsistent with the predictions of models for phase slip via homogeneous defect nucleation, and provide evidence for amplitude defect motion. The presence of substantial amounts of phase slip at large distances from the current contacts explains the loss of coherence of the sliding CDW observed at lower temperatures, and suggests that predictions of phase-only models of CDW dynamics may be of very limited use in describing the sliding CDW in $NbSe_3$. [S0163-1829(98)02020-7]

I. INTRODUCTION

The charge-density wave (CDW) ground state exhibited by quasi-one-dimensional conductors such as $NbSe_3$ consists of a modulation of the conduction electron density $n(x,t) = n_0 + \delta n \cos[Qx + \theta(x,t)]$ and a concomitant modulation of the positions of the lattice atoms.[1] When an electric field greater than a threshold field E_T is applied, the CDW can depin from impurities and move through the crystal, resulting in collective charge transport. CDW motion gives rise to a host of unusual phenomena that are a consequence of the interactions of the CDW's many degrees of freedom with the random field due to impurities. Analogous phenomena are exhibited by superconducting flux lattices, magnetic materials, fluids in porous media, and by systems with moving interfaces.[2] CDW conductors often show the phenomena more cleanly, and thus have been considered prototypical systems for study of collective dynamics in the presence of disorder.

Conventional models of CDW dynamics describe the CDW as an overdamped elastic medium in a random potential, and assume that the phase $\theta(x,t)$ of the CDW's order parameter is continuous while its amplitude is constant.[3] These models predict that above threshold the CDW state should evolve periodically with a period $\tau = \lambda_c / v_c$, and that it should exhibit critical behavior as the applied field approaches the depining field from above.[4–6] Neither perfect periodicity nor clear evidence for critical behavior has been observed experimentally.

CDWs are not perfectly elastic. They exhibit amplitude defects and associated discontinuities of the CDW phase that correspond to dislocations of the CDW superlattice, and these give rise to plastic behavior.[7] CDW defects are in fact essential for steady CDW motion to occur at all. As there is no analog to Andreev scattering,[8] only quasiparticles can be injected at current contacts, and quasiparticle charge must be converted to CDW condensate charge in the bulk. Theoretical work[9–11] has suggested that this conversion occurs via a phase-slip process in which dislocation loops form and grow in the CDW superlattice, leading to addition and removal of CDW phase fronts in a process analogous to phase slip in superconductors[12] and superfluids.[13] When an electric field E greater than the bulk threshold field E_P is applied between current contacts, the CDW slides from one contact towards the other. The CDW becomes compressed near one contact and stretched near the other,[14,15] and the resulting strain $\epsilon(x) \equiv (1/Q)(\partial\theta/\partial x)$ reduces the barrier energy to formation of dislocation loops. The dislocation formation rate is largest near the current contacts, where $|\epsilon|$ is largest. The local phase-slip rate,

$$r_{ps}(x) = -(Q/en_c)\partial j_c/\partial x, \tag{1}$$

where n_c is the CDW carrier concentration and $-e$ is the electronic charge, is determined by the rate at which dislocation formation and motion removes or adds CDW phase fronts near each contact. The integral of this rate determines the CDW current profile $j_c(x)$, as illustrated in Fig. 1.

Experiments on the CDW conductor $NbSe_3$ using a four-probe configuration[16,17] measured the phase-slip rate integrated over half of the sample versus a ''phase-slip voltage'' V_{ps} related to the average magnitude of the strain between the current contacts,[18] and found good agreement with the predictions of a model for phase slip via homogeneous thermal nucleation of dislocation loops.[11] A subsequent four-probe experiment[19] was, however, interpreted as evidence

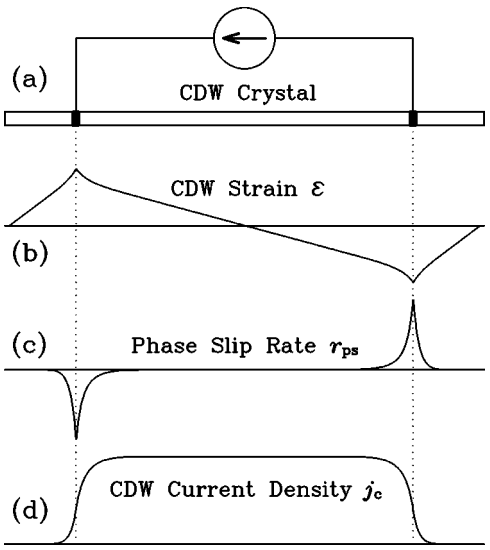

FIG. 1. Relation between the CDW strain $\epsilon(x)$, the phase-slip rate $r_{ps}(x)$, and the CDW current density $j_c(x)$. In (a), a current density j_{tot} greater than j_T, the threshold for nonlinear conduction, is injected into a $NbSe_3$ whisker at side contacts. This causes the CDW to become compressed near one contact and stretched near the other; the resulting macroscopic CDW strain field $\epsilon(x) \propto (\partial\theta/\partial x)$ is shown in (b). Phase fronts are added or removed through phase slip in the regions near the contacts where $|\epsilon(x)|$ is large, resulting in a local phase-slip rate $r_{ps}(x)$ as shown in (c); the spatial integral of $r_{ps}(x)$ gives the CDW current density $j_c(x)$, shown in (d). The polarity of $\epsilon(x)$ and $r_{ps}(x)$ shown here corresponds to an electronlike CDW such as the T_{P_1} CDW of $NbSe_3$.

that phase slip occurs at substantial distances from the current contacts, contrary to the model's prediction. Spatially resolved measurements on $NbSe_3$ using an array of contacts also detected evidence for phase-slip-induced disturbances hundreds of micrometers from the current contacts.[20] The results of the latter experiment were, however, corrupted by contact perturbations, and the actual phase-slip profile could not be determined. Recent spatially resolved studies on $K_{0.3}MoO_3$ using a novel electro-optical technique have yielded high-resolution measurements of the CDW strain profile and its response to changes in the driving current direction.[22] Unfortunately, contact perturbations and the large anisotropy of this material have made measurements of the corresponding phase-slip profile difficult.

Here we report spatially resolved measurements of the CDW current distribution $j_c(x)$ in $NbSe_3$ performed using micrometer-scale nonperturbing electrodes. These measurements confirm that substantial phase slip can occur more than 100 μm from current contacts at temperatures well below the CDW transition temperature. We analyze the current distributions to yield the profiles of both the CDW strain $\epsilon(x)$ and the phase-slip rate $r_{ps}(x)$, and combine these profiles to obtain the local relation between phase-slip rate and strain. This relation is not unique but varies with distance from the current contacts, providing evidence for dislocation motion. The observed phase-slip profiles explain the loss of coherence of the sliding CDW observed with decreasing temperature, and suggest that the plastic behavior of real CDWs may render important predictions of elastic CDW models untestable. Some preliminary results have been reported previously.[23]

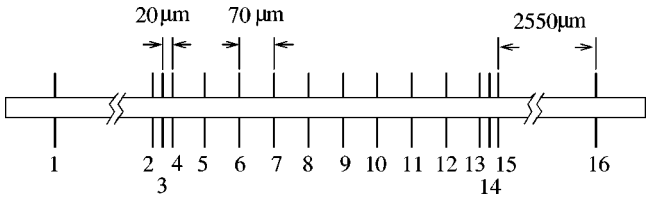

FIG. 2. Measurement geometry. Unless noted otherwise, a current density j_{tot} was injected at contacts 2 and 15 and the voltage measured across the remaining pairs of adjacent contacts [(3,4), (4,5), . . . , (13,14)]. Electrodes 1 and 16 are 50 μm wide; all others are 2 μm wide.

II. EXPERIMENTAL METHODS

The present measurements were made possible by a method for obtaining high-quality nonperturbing contacts to single-crystal whiskers of $NbSe_3$ described by Adelman *et al.*[23] High-purity crystals (bulk $r_R \approx 300$) were placed on alumina substrates patterned photolithographically with fine gold-topped chromium wires (1.5–2.0 μm wide, 0.1 μm high), and then held in place by a thin polymer film. Similar patterned substrates have been used by previous investigators,[20,24] but the polymer film improves contact reliability and permits narrower contacts. The geometry used is shown in Fig. 2. As will be discussed in Sec. IV F, these contacts were essentially nonperturbing at temperatures well below the CDW transition temperature. The dimensions of the samples reported upon here are given in Table I.

CDW current profiles were measured by injecting a dc current density j_{tot} through two contacts (2 and 15 in Fig. 2 unless otherwise noted) and measuring the voltage across the remaining pairs of adjacent contacts. A smaller current density $j_{tot} = 0.1 - 0.25 j_T$, where j_T is the threshold current density corresponding to E_T, was used to determine the low-field resistance R_n due to quasiparticle conduction of each of the segments. The average CDW current density in each segment was then calculated by subtracting the quasiparticle contribution to the total current density as $\langle j_c \rangle = j_{tot} - \langle j_n \rangle = j_{tot} - A^{-1} V(j_{tot})/R_n$. Current profiles for the $T_{P_1} = 145$ K CDW were recorded for driving currents up to about five times j_T and for temperatures between 70 and 135 K.

The calculation $\langle j_c \rangle = j_{tot} - A^{-1} V(j_{tot})/R_n$ assumes that R_n is independent of j_{tot}. If this is not the case and $R_n = R_n^0 + \delta R_n(j_{tot})$, then the calculated j_c will be in error by $\delta j_c \approx -j_n(\delta R_n / R_n^0)$. Measurements and calculations indi-

TABLE I. Dimensions and threshold current densities for the samples used herein. The sample cross-sectional area was evaluated from the room-temperature resistance using $\rho(300\text{ K}) = 1.85 \pm 0.03$ Ω μm. j_T is given for $T = 90$ K using contacts 2 and 15 for current injection. The listed uncertainties are dominated by the uncertainty in $\rho(300\text{ K})$.

No.	Cross section A (μm^2)	Thickness t (μm)	j_T at 90 K (μA/μm^2)
1	10.3±0.2	1.7±0.2	13.6±0.2
2	18.4±0.3	1.9±0.2	12.5±0.2
3	11.4±0.2	1.9±0.2	18.0±0.3
4	7.3±0.1	1.2±0.1	19.2±0.3

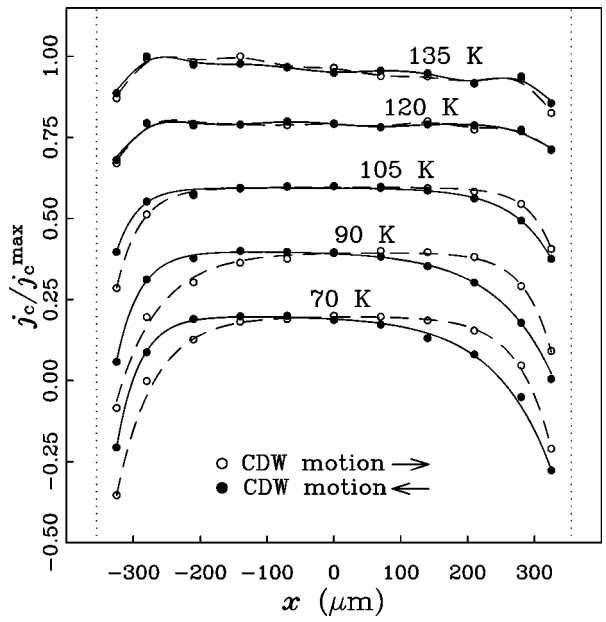

FIG. 3. CDW current density $j_c(x)$ vs temperature for sample 1. The driving current density j_{tot} was varied such that $j_c = 8.3\ \mu A/\mu m^2$ at the center of the sample for all temperatures. This CDW current density corresponds to a driving current $j_{tot}=4.3j_T$ at $T=90$ K. For clarity, curves are shown normalized to their maximum value and successive curves are shifted down by 0.2. The connecting lines for $T=135$ K and $T=120$ K are guides to the eye and for $T=105$ K, $T=90$ K, and $T=70$ K they are fits to Eq. (2). The dotted vertical lines indicate the positions of the current contacts at $x=\pm L/2=355\ \mu$m.

cate that such errors introduced by CDW strains, bulk Joule heating, and by fringing near the current contacts are small for all data presented here.[25] A more significant source of error is Joule heating at the current contacts' Au-$NbSe_3$ interface due to the finite contact resistance. Measurements indicate that the size of the heated region is less than the 20 μm resolution of our experiments, and that the $NbSe_3$ region immediately adjacent to the Au/Cr contact may experience more than 10 times as much heating as the bulk. If the regions near the current contacts are at a higher temperature, a smaller strain will be required to generate phase slip there, and this in turn will result in a reduced strain $\epsilon(x)$ and a modified CDW current profile everywhere between the current contact — even though most of this region is not heated. This effect limited the maximum current density that yielded reliable data in our experiments to about $5j_T$ at 90 K.

III. EXPERIMENTAL RESULTS

A. Dependence of $j_c(x)$ on temperature

Figure 3 shows typical CDW current profiles $j_c(x)$ at several temperatures. For all profiles, the CDW current is smaller near the current contacts than near the center of the sample. At 135 K and 120 K, j_c is appreciably reduced only in the immediate vicinity (within $\approx 30\ \mu$m) of the current contacts; at 105 K, the regions of reduced j_c extend more than 100 μm from the current contacts. At 90 and 70 K, $j_c(x)$ has a finite slope everywhere, indicating that phase slip is occurring in the entire region between the current contacts. Effects of voltage contact perturbations on these profiles are significant in the $T=135$ K and 120 K data, where they cause a larger reduction of j_c near the current contacts than would be obtained with nonperturbing contacts.

An interesting feature of the profiles for $T<120$ K is a consistent asymmetry with respect to driving current polarity. The CDW current is greater near the positively biased current contact — the region where the CDW is compressed and phase fronts are being removed by phase slip — than near the negative contact. The asymmetry $[j_c(x,j_{tot})-j_c(x,-j_{tot})]/2$ grows roughly linearly with distance from the midpoint between the current contacts ($x=0$ in Fig. 3). The magnitude of the asymmetry is negligible above 105 K, and grows to a value of $[j_c(x_0,j_{tot})-j_c(x_0,-j_{tot})]\approx 0.06j_c(0,\pm j_{tot})$ at 70 K at a point x_0 half-way from $x=0$ to the current contacts.

The profiles at 70, 90, and 105 K in Fig. 3 are fitted to the empirical form

$$j_c(x)=j_0-j_1\ \exp\left[-(L/2+x)/l_1\right] - j_2\ \exp\left[-(L/2-x)/l_2\right], \tag{2}$$

where L is the distance between the current contacts and $x=0$ is the midpoint between them.

B. Dependence of $j_c(x)$ on driving current

Figure 4 shows the dependence of the CDW current profile on driving current density j_{tot} at $T=90$ K. The ratio of the CDW current near the current contacts to its mid-sample value increases with increasing j_{tot}. The extent of the region over which phase slip occurs can be characterized by a phase-slip length l_s, calculated as

$$l_s=\frac{en_c}{Qj_c^{max}}\int_{x_0}^{x(j_c^{max})}(x-x_0)\ r_{ps}(x)\ dx. \tag{3}$$

Here x_0 is the position of a current contact and $x(j_c^{max})$ is the position where $j_c(x)$ is a maximum. Figure 5 shows the dependence of l_s on the maximum CDW current j_c^{max} at 90 K, with results for the positively and negatively biased contacts plotted separately. The phase-slip length l_s decreases monotonically with increasing CDW current, reflecting the decreasing curvature of the profiles of Fig. 4(b).

C. Dependence of $j_c(x)$ on current contact separation

Figure 6 shows $j_c(x)$ for several current contact separations L at fixed j_c^{max} and $T=90$ K. Contact 2 was used as one current contact in all the profiles; contacts 6 through 15 were successively used as the second current contact, yielding values of L from 180 to 710 μm. Profiles measured with negative currents are plotted as $-j_c(-x)$ in Fig. 6, providing the data near $x/L=1$.

The profiles corresponding to different L have essentially the same functional form, $j_c(x,L)=f(x/L)$. Only the CDW current densities measured at the voltage contact pairs nearest to the current contacts deviate significantly from this relationship. Similar behavior was observed at 70 and at 105 K; at 120 and 135 K the small size of the phase-slip regions and contact perturbations prevent meaningful comparison.

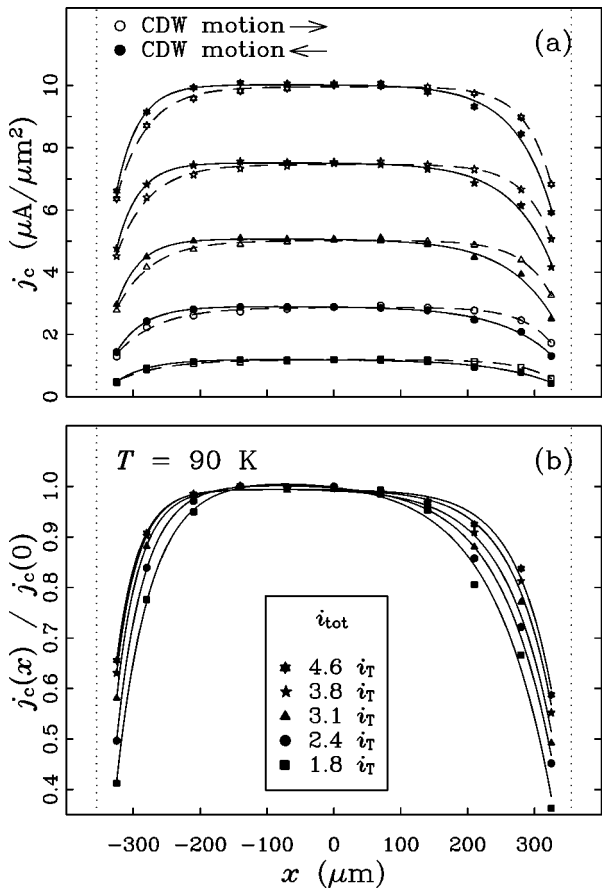

FIG. 4. CDW current density $j_c(x)$ vs driving current density $j_{\rm tot}$ at $T=90$ K for sample 2. In (a), $j_c(x)$ is plotted for both polarities of the driving current. In (b), $j_c(x)$ is normalized to unity at midsample and plotted only for positive $j_{\rm tot}$. The relative curvature of the profiles increases with decreasing driving current. The connecting lines are fits to Eq. (2); the dotted vertical lines indicate the positions of the current contacts.

D. CDW current beyond the current injection contacts

The macroscopic CDW strain profile due to an applied electric field between the current contacts must, because of elastic interactions, extend beyond the current contacts.[18,23,26] Consequently, some phase slip and CDW conduction are expected in those regions. Since the net current beyond the current contacts is zero, the CDW current must be balanced by the normal current due to quasiparticle flow, $j_n=-f$, resulting in an electric field $E(x)=-\rho_n j_c(x)$.

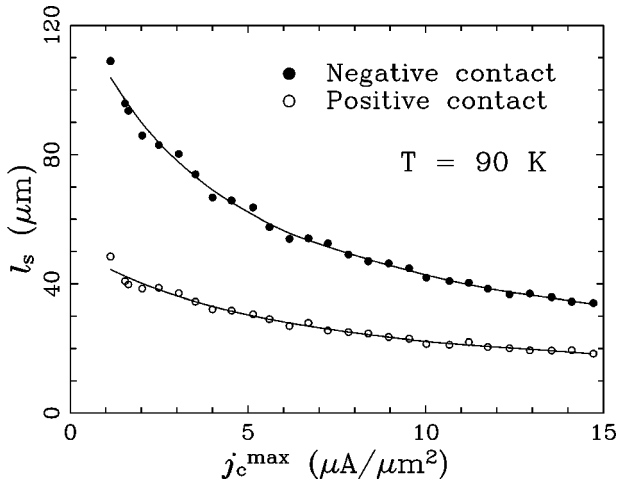

FIG. 5. Characteristic size l_s of the phase-slip region near the current electrodes, as defined in Eq. (3), for sample 1 at 90 K. l_s is larger for the negative contact, reflecting the asymmetry in the CDW current profiles.

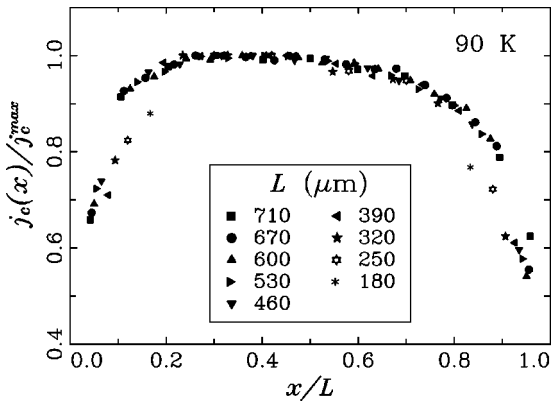

FIG. 6. CDW current density $j_c(x)$ for nine current contact separations L, measured in sample 1 at 90 K with a constant midsample CDW current density $j_c = 8.8\ \mu$A/μm^2. The abscissa is scaled for each profile such that $x/L=0$ and $x/L=1$ correspond to the positions of the current contacts. Note that the data obey $j_c(x,L)=f(x/L)$ near the center of the sample; only the endmost points of each curve, located 30 μm from a current contact, depart from this relationship.

This electric field due to CDW motion beyond current contacts was measured by injecting a current through electrodes 1 and 2 and measuring the voltage across electrodes 3 and 4. The average CDW current in segment (3,4) at $T=90$ K was 2% of the CDW current between the current contacts. No voltage was detected across contacts 4 and 5. Consequently, phase slip must be confined to a region extending less than 40 μm beyond the current contacts.

E. Mode locking and the CDW velocity profile

The discussion of the data of Figs. 3–6 has implicitly assumed that the observed variations in $j_c=en_cv_c$ are due to changes in v_c and not to changes in the effective n_c resulting from filamentary conduction. This assumption could be tested by measuring the frequency of the coherent oscillations (''narrow-band noise'') that accompany dc CDW current flow. These oscillations are analogous to those of the ac Josephson effect, and arise due to periodic interaction of the CDW with impurities. By measuring the oscillation frequency $\omega_c=Qv_c$ versus position, the CDW velocity profile $v_c(x)$ could be obtained directly. Unfortunately, a direct measurement of the oscillations was hampered by the relatively high series resistance of the micrometer-scale contacts. Instead, the velocity profile was probed by mode locking the frequency ω_c to an applied ac frequency $\omega_{\rm ac}$ to produce steps (analogous to Shapiro steps) on the j_c–$j_{\rm dc}$ characteristic where j_c remained nearly constant over some finite range of $j_{\rm dc}$.

Figure 7 shows the measured dV/dI versus position at $T=105$ K.[27] Steps of nearly constant CDW current appear as peaks in dV/dI; these peaks shift to higher driving currents

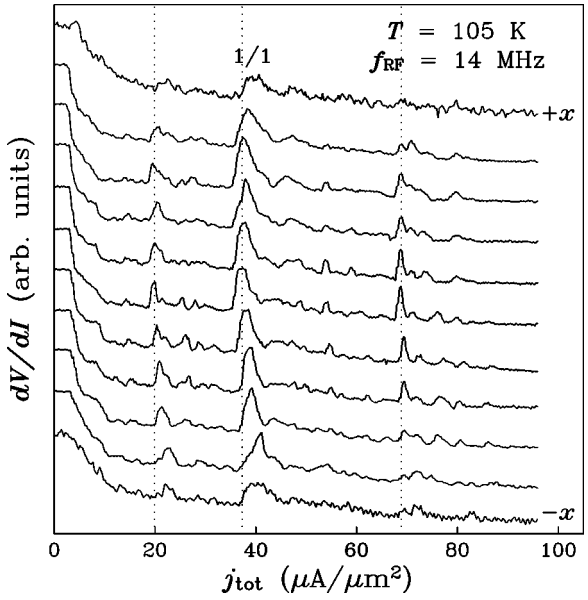

FIG. 7. CDW mode locking to an applied 14-MHz sinusoidal excitation. Each curve gives dV/dI at a pair of adjacent voltage contacts, the bottom curve corresponding to pair (3,4) and the top curve to pair (13,14). The dotted vertical lines identify the 1/2, 1/1, and 2/1 mode-locking steps. These steps shift to higher currents for positions closer to the current contacts, consistent with the observed $j_c(x)$ profiles. The data are from sample 3 at 105 K.

$j_{\rm dc}$ as the current contacts are approached. This indicates that it takes a larger driving current to achieve a given ω_c and CDW velocity v_c near the current contacts and that, for a given driving current, the CDW velocity is smaller near the current contacts. This supports the assumption that the measured CDW current profiles $j_c(x)$ do indeed reflect changes in the CDW velocity.

IV. ANALYSIS AND DISCUSSION

A. The slip-strain relation

The current profiles of Figs. 3–6 can be analyzed to obtain the corresponding phase-slip profiles $r_{\rm ps}(x)$, the strain profiles $\epsilon(x)$, and thus the local relationship between phase-slip rate and strain. From the definition of Eq. (1), the phase-slip rate $r_{\rm ps}(x_n)$ at the position of the nth voltage contact x_n can be calculated as

$$r_{\rm ps}(x_n)\approx -\frac{Q}{en_c}\frac{2}{x_{n+1}-x_{n-1}}(\langle j_c\rangle_{n+1,n}-\langle j_c\rangle_{n,n-1}), \quad (4)$$

where $\langle\ \rangle_{nm}$ denotes an average from x_m to x_n. The accuracy of the approximation in Eq. (4) and minor corrections to it are discussed in the Appendix. For the voltage contacts immediately adjacent to the current contacts, Eq. (4) does not apply and we take $r_{\rm ps}\propto\langle j_c\rangle$.

The macroscopic strain profile $\epsilon(x)$ can be calculated from measured CDW current profiles using the method discussed by Adelman *et al.* A simplified one-dimensional model is used in which the effects of pinning are accounted for phenomenologically using an experimentally determined pinning force $E_P(j_c)$. In the steady state, the model is described by the equation of motion

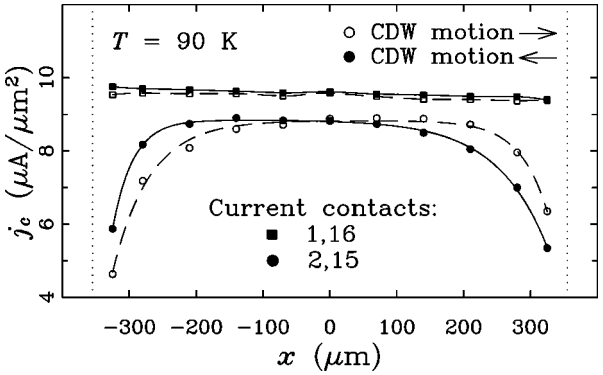

FIG. 8. CDW current density profile $j_c(x)$ in sample 1 at 90 K for current injection at contacts 2 and 15 (circles) and at contacts 1 and 16 (squares). $j_c(x)$ is essentially position independent in the latter case, suggesting that the voltage electrodes are not perturbing the profile appreciably. Although all profiles are for $j_{\rm tot}=61\ \mu{\rm A}/\mu{\rm m}^2$, $j_c(x)$ is greater when injecting current at contacts 1 and 16 since the elastic force $\propto(\partial\epsilon/\partial x)$ due to the macroscopic strain field is smaller in this case.

$$j_c(x)=\frac{1}{\rho_n+\rho_c}\left[\rho_n j_{\rm tot}(x)-E_P(j_c)+\kappa\frac{\partial\epsilon(x)}{\partial x}\right] \quad (5)$$

$$=-\frac{en_c}{Q}\int_{-\infty}^{x} r_{\rm ps}(x')dx', \quad (6)$$

where $\rho_c=\gamma(Q/en_c)^2$ is the high-field CDW resistivity, γ is a phenomenological CDW damping constant, $\kappa\equiv(Q^2/en_c)K$, and K is the longitudinal CDW elastic constant. This model reproduces most features of the experimental spatiotemporal response of the CDW in $NbSe_3$ to bipolar current pulses.

The strain profile can be determined using Eq. (5) from measurements of the current profiles $j_c^0(x)$ and $j_c^1(x)$ obtained by injecting the same driving current through contact pairs (1,16) and (2,15), respectively. The elastic force $\propto\kappa(\partial\epsilon/\partial x)$ for a given driving current scales roughly inversely with current contact separation. Consequently, for widely separated current contacts the elastic force is small, and the profile $j_c^0(x)$ is determined by $j_{\rm tot}$ and $E_P(j_c)$ only. Figure 8 shows sample data at 90 K. $j_c^0(x)$ is essentially independent of x since the current contacts are far from the voltage contacts, and is larger than the maximum value of j_c^1 since the elastic force is much smaller in the former case. It follows from Eq. (5) that the strain at the position of each voltage contact is given by

$$\epsilon(x_n)=\epsilon(x_0)+\frac{\rho_c+\rho_n}{\kappa}\sum_{m=1}^{n}L_{m,m-1}\times\left\langle j_c^1-j_c^0+\frac{E_P(j_c^1)-E_P(j_c^0)}{\rho_c+\rho_n}\right\rangle_{m,m-1}. \quad (7)$$

By approximating $\langle E_P(j_c)\rangle\approx E_P(\langle j_c\rangle)$, which is valid since E_P changes slowly with x, all terms on the right-hand side except the constant $\epsilon(x_0)$ can be determined experimentally.

Figure 9 shows the phase-slip rate $r_{\rm ps}$ versus $1/\kappa\epsilon$ at $T=90$ K as calculated from Eqs. (4) and (7) for several distances x from the current injection contacts. The two current

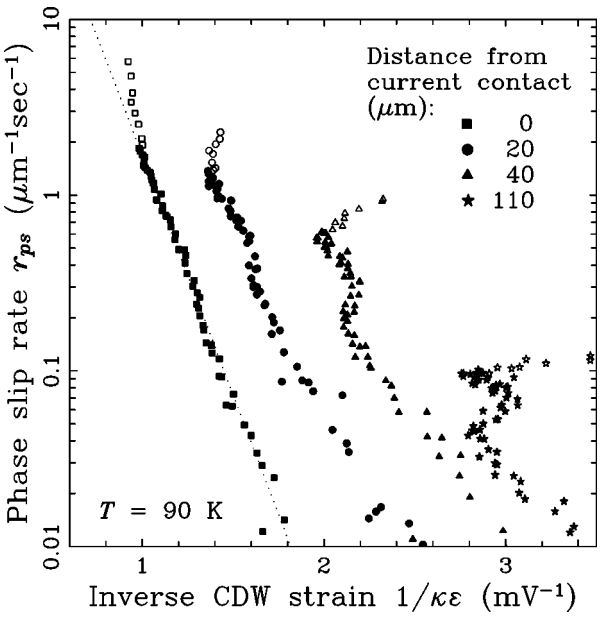

FIG. 9. Phase-slip rate $r_{ps}(x)$ vs CDW strain $\epsilon(x)$ at four positions x in sample 4 at $T=90$ K. Each data point corresponds to a different driving current. According to the bulk nucleation model, Eq. (8), the data for the various positions should collapse onto a unique straight line. Instead, r_{ps} for a given ϵ increases with distance from the current contact. The dotted line is a fit of the $x=0$ data to Eq. (8).

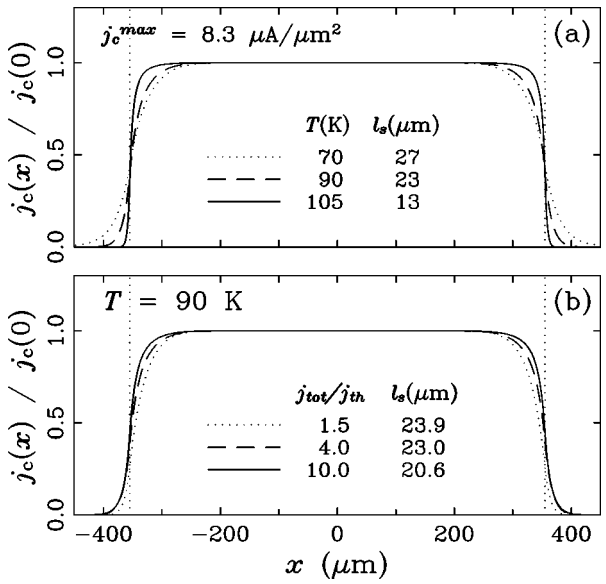

FIG. 10. Simulated CDW current profiles $j_c(x)$ using Eq. (5) for the equation of motion, the bulk nucleation model [Eq. (8)] for the phase slip rate, and material parameters corresponding to sample 1. (a) shows the dependence of $j_c(x)$ on temperature at fixed maximum CDW current density $j_c=8.3\ \mu\text{A}/\mu\text{m}^2$. (b) shows the dependence of $j_c(x)$ on driving current at $T=90$ K. Although the simulations reproduce qualitatively the experimental dependence on temperature and driving current, they show no asymmetry and predict phase-slip regions that are smaller than in the experiment.

polarities were averaged together[28] and $\epsilon(x_0)$ chosen to produce $\epsilon=0$ at the center of the sample. At all positions the phase-slip rate increases rapidly with increasing strain. However, for a given strain the phase-slip rate grows with increasing distance from the current contacts. The curves for $x>0$ exhibit kinks that are similar from curve to curve and are reproducible for a given sample, but vary from sample to sample. They can be traced to irregularities in $\epsilon(x,j_{\text{tot}})$ in the middle part of the sample that are propagated through the summation of Eq. (7). For large applied currents (as indicated by the open symbols in Fig. 9), the strain for a given slip rate is reduced due to heating in the immediate vicinity of the current contacts, as discussed in Sec. II.

B. Comparison with the homogeneous nucleation model of phase slip

The only quantitative predictions for CDW phase slip have been made by Ramakrishna *et al.*,[11] based on earlier work by Maki[9] and by Feinberg and Friedel.[10] In their model, dislocation loops form in the presence of CDW strain by homogeneous thermal nucleation, and then grow by climb to remove or add an entire CDW phase front. Assuming that the local phase-slip rate is simply proportional to the local nucleation rate, they predicted that

$$r_{\text{ps}}(x) = -\,\text{sgn}[\,\epsilon(x)\,]\; r_0\; e^{-V_a/2\kappa|\epsilon(x)|}, \tag{8}$$

where $V_a \approx \zeta(\pi^2 Q/en_c)(\overline{K}/k_B T)$, ζ is a constant of order unity, $\overline{K}=[(K_x K)^{1/2}+(K_y K)^{1/2}]/2$ is a normalized transverse elastic constant, K is the longitudinal elastic constant, and r_0 is related to an attempt rate that is difficult to estimate.

The dotted line in Fig. 9 shows a fit of Eq. (8) to the r_{ps}-ϵ data near the current contact ($x=0$). The predicted functional form is consistent with the data over the full two decade range of r_{ps}. The fit yields $r_0=2\times10^{15}$ and $V_a=19$ mV; data from the other samples in Table I give V_a ranging from 17 to 23 mV.

Previous four-probe measurements[18] were analyzed to obtain the total phase-slip rate versus a quantity V_{ps} related to the average strain. Those data were well described by the corresponding homogeneous nucleation theory prediction, most likely because the total phase-slip rate in four-probe measurements is dominated by slip near the current contacts. The value of r_0 obtained here is in good agreement with those results, but the value of V_a is smaller than Maher *et al.*'s estimate of 35 mV at 90 K. As pointed out by Adelman *et al.*,[23] however, the value of V_a obtained from the four-probe measurements was overestimated because of simplifications[29] made in interpreting the meaning of V_{ps}.[30]

Away from the current contacts, the observed slip-strain relation deviates from the prediction of the homogeneous nucleation theory in a fundamental way: the relation is not unique, but varies with position. As noted above, the slip rate for a given strain increases with increasing distance from the contact. The data for $x>0$ roughly follow the activated form of Eq. (8) with an activation energy that is comparable to that of the $x=0$ curve, but with an r_0 that increases by an order of magnitude for each 20 μm of distance from the current contacts.

Equation (8) for $r_{\text{ps}}(\epsilon)$ due to homogeneous nucleation can be combined with the model of Eq. (5) to predict the CDW current profile $j_c(x)$. Figure 10 shows simulated j_c profiles using the material parameters of sample 1.[31] The

calculated profiles reproduce qualitative features of the experiment, including the decrease in the size of the phase-slip region with increasing temperature and with increasing driving current. The simulated slip regions are too small, however, because the homogeneous nucleation model underestimates the amount of slip for a given strain away from the current contacts.

The origin of the discrepancy between our measurements of $r_{ps}(x)$ away from the current contacts and Eq. (8) is not known. One possibility is that the additional phase slip is due to dislocation motion along the direction of current flow, as has been discussed by Gill.[19,35] The derivation of Eq. (8) assumes that dislocations grow and add or remove phase fronts where they are nucleated. But dislocations can move with the moving CDW as they grow, and in the presence of shear stresses such as those associated with field fringing at current contacts or with variations in crystal thickness across the crystal width[32] they can glide along the CDW as well. Although simple estimates and measurements of the transient response of the CDW indicate that the first mechanism is not significant,[23] the second could result in substantial slip occurring far from the contacts where the strains are too small to produce appreciable nucleation. The discrepancy between the measured and predicted slip-strain relations could also arise because dislocations form by some other mechanism (although this mechanism should exhibit a strong variation of rate with strain), because of dislocation-dislocation interactions, or because of the effects of the fluctuating strains associated with the moving CDW's interaction with impurities.[5,6,33]

C. Source of the asymmetry in $j_c(x)$

A surprising feature of the CDW current profiles is their asymmetry with respect to the driving current direction. Equation (5) for j_c together with Eq. (8) for $r_{ps}(\epsilon)$ predict that $j_c(x)$ is symmetric and $\epsilon(x)$ is antisymmetric about the midpoint between the current contacts. At 70 and 90 K, however, $j_c(x)$ has an antisymmetric component that is about 3% of its symmetric component and $\epsilon(x)$ has a symmetric component that is about 10% of its antisymmetric component. Similar asymmetries have been observed in the semiconducting materials TaS_3 (Ref. 21) and $K_{0.3}MoO_3$.[34]

The asymmetry in $j_c(x)$ can be described phenomenologically by introducing an additional term in the CDW equation of motion. The lowest order term with the proper symmetry is obtained by replacing $\kappa(\partial\epsilon/\partial x)$ by $\kappa(\partial\epsilon/\partial x) + \mathrm{sgn}(j_c)\beta\epsilon$ in Eq. (5). Gill suggested a formally equivalent model to account for an asymmetry in the response to nonuniform driving fields.[35,36] Several mechanisms can give rise to such a term to leading order, including the modulation of the single-particle resistivity by the CDW strain, nonharmonicity in the elastic energy due to electron-hole asymmetry, and a dependence of the CDW damping constant γ on the local CDW wave vector $Q(1+\epsilon)$.

Postulating that such a term is responsible for the observed asymmetry, we estimate the value of the parameter β. The strain profile $\epsilon(x;j_{tot},\beta)$ can be calculated as a function of β from our experimental CDW current profiles.[37] Since we are assuming that the observed asymmetry is not due to the phase-slip process, the magnitude of $r_{ps}(\epsilon,x)$ is independent of $\mathrm{sgn}(\epsilon)$ for a given distance from the current contacts; it follows that the correct value of β is that for which the curves $r_{ps}(\epsilon)$ for all symmetrically positioned pairs of voltage contacts (e.g., pairs 3–4 and 13–14) collapse onto each other simultaneously. This procedure yields $\beta/\kappa=(1.0\pm0.5)\times10^{-3}\ \mu\mathrm{m}^{-1}$ at 90 K. For comparison, the modulation of the single-particle resistance by the CDW strain[38] gives a value $\beta/\kappa\approx5\times10^{-6}$ for typical driving current densities, which is too small by two orders of magnitude. Similarly, a modulation of the elastic constant or damping constant of the order of 10% would be required to cause the observed asymmetry, far greater than can be expected from the change in the CDW wave vector of order 0.1% that results from the macroscopic strain field.

It therefore seems likely that the observed asymmetry is not a property of the elastic CDW, but rather is a consequence of the phase-slip process. The shape of the observed CDW current profiles is determined by the phase-slip rate far from the current contacts, and this rate is not accounted for by existing models of phase slip. This suggests that a characteristic feature of the mechanism that leads to the excess phase slip is sensitivity to the polarity of the driving electric field.

D. Consequences of the observed $j_c(x)$

Aside from their importance in elucidating the mechanism underlying phase slip and current conversion in CDW conductors, the present results explain some previously puzzling observations and have broader implications as well. In $NbSe_3$, the spectral width of the coherent oscillations that accompany dc current flow increases rapidly when the temperature is decreased below 120 K, and the fundamental spectral peak develops a low-frequency tail. The mode-locking steps on the dc I-V characteristic become rounded, the corresponding peaks in dV/dI become broadened and reduced in amplitude, and most subharmonic peaks disappear entirely.[39] In addition, the onset of CDW conduction at threshold becomes progressively more gradual.[40] These results are inconsistent with purely elastic models of CDW's, which predict a vanishing spectral width for the coherent oscillations, sharp mode-locking features, and a single form for the dc I-V characteristic over a broad temperature range.

The observed behavior is a consequence of the evolution of the CDW current profile with temperature. The width of the region near the current contacts where the CDW current is below its midsample value $j_c^{\max}$ grows rapidly below 120 K. The CDW moves more slowly in these regions, producing a distribution of coherent oscillation frequencies below the fundamental spectral peak corresponding to $j_c^{\max}$. This distribution of velocities and coherent oscillation frequencies leads to rounding of the $\langle j_c\rangle$-V characteristic, particularly near threshold or in short specimens, and to rounding of the mode-locked steps, as is evident in Fig. 7. The detailed effects on mode-locking behavior are likely quite complicated, since there is presumably competition for locking of adjacent regions with different preferred coherent oscillation frequencies to different rational multiples of the applied ac frequency. All of these effects are observed even in four-probe measurements because the voltage contacts used in standard

measurements are always heavily perturbing and the current they shunt out of the crystal must be reinjected via phase slip.

The present results also have ramifications for the analysis of experiments measuring the dynamical CDW carrier density. n_c can be determined from the relationship between CDW current density and fundamental coherent oscillation frequency as $n_c=(Q/e)(dj_c/d\omega_c)$. Richard, Chen, and Artemenko[41] found that $d\langle j_c\rangle/d\omega_c$ decreases with decreasing temperature at temperatures well below T_p, contrary to expectations. McCarten *et al.*[42] argued that this effect is due to interactions between the normal carriers and the sliding CDW. The analysis of the experiment, however, assumes that $j_c(x)$ is constant. Since the low-frequency tail is normally ignored in determining ω_c from the coherent oscillation spectrum, the measured ω_c corresponds to $j_c^{\max}$, the CDW current density in the region far from the contacts. The dip in $j_c(x)$ near the current contacts at low temperatures thus reduces $\langle j_c\rangle$ but not ω_c, leading to an apparent reduction in n_c. The fractional reduction is predicted to be of the order of $2l_s/L$, the ratio of the length of the phase slip regions to the sample length. This is consistent with the reported order of magnitude of the effect.

Dynamical critical behavior predicted based on elastic models of the CDW has been the focus of much of the theoretical attention devoted to CDW's for more than a decade.[4–6] Various experiments have attempted to confirm predicted scaling forms for the dc *I-V* characteristic just above threshold[43] and near the edges of mode-locked steps.[44] The present results showing that substantial phase slip occurs over large distances in $NbSe_3$ imply that these predictions, being based on purely elastic models, are experimentally irrelevant. Coppersmith[45] has pointed out that for sufficiently large systems, elastic models exhibit local regions with very large CDW strain and thus must fail due to phase slip. While this observation is of fundamental importance, the effects of phase slip at current contacts on observed properties is many orders of magnitude larger.

E. Determining the phase-slip distribution in other materials

The CDW current profiles in other CDW materials, including TaS_3 and $K_{0.3}MoO_3$, have not been determined. This is due in part to the difficulty of forming high-quality nonperturbing contacts to these materials. More importantly, unlike $NbSe_3$ these materials are fully gapped below the CDW transition and have much smaller single-particle densities. As a result, the effects of CDW strains on the single-particle resistance are much larger, and the simple separation of CDW and single-particle currents using Eq. (5) is not a good approximation.

Itkis *et al.*[22] have succeeded in measuring the CDW strain profile $\epsilon(x)$ in $K_{0.3}MoO_3$ versus driving current by measuring the modulation of the infrared absorption by CDW strain. Using the model of Adelman *et al.*, these results can be analyzed to estimate the phase-slip distribution. Combining the definition of $r_{ps}(x)$, Eq. (1), and the CDW equation of motion, Eq. (5), and assuming that $dE_P[j_c(x)]/dx\approx 0$ yields

$$r_{ps}(x)\approx -\frac{Q\kappa}{en_c(\rho_n+\rho_c)}\frac{\partial^2\epsilon(x)}{\partial x^2}. \tag{9}$$

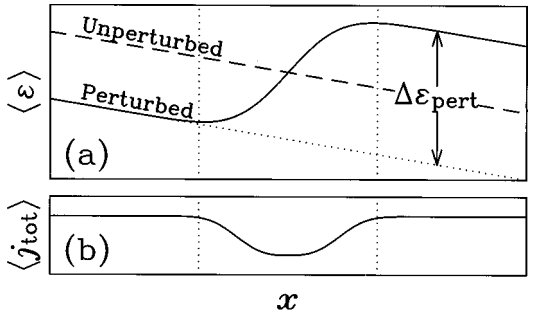

FIG. 11. Schematic illustration of perturbation by a voltage contact. In (a), the dashed line represents the macroscopic strain field $\epsilon(x)$ in the vicinity of a voltage contact (delimited by the vertical dotted lines) in the absence of contact perturbations. Shunting by the contact reduces the average current density $\langle j_{tot}(x)\rangle$ in the sample cross section, as shown in (b). For a small perturbation, only the quasiparticle current density $\langle j_n\rangle$ is reduced while the CDW current density $\langle j_c\rangle$ remains constant; the reduced electric field $\rho_n\langle j_n\rangle$ is compensated by a change in the CDW strain gradient near the contact [solid line in (a)]. The contacts become perturbing when $\Delta\epsilon_{pert}$, as shown in the figure, becomes comparable to $\Delta x\,(\partial\epsilon/\partial x)_{macro}$, the change in strain due to the macroscopic strain field between a current contact and the adjacent voltage contact.

Applying[46] Eq. (9) to the data of Itkis *et al.* yields a phase-slip region in $K_{0.3}MoO_3$ with a width on the order of 100 μm, comparable to what is observed in $NbSe_3$. This suggests that many of the conclusions drawn here should be applicable to other CDW materials.

F. Contact perturbations

Previous attempts to measure CDW current profiles in $NbSe_3$ and other materials were unsuccessful because of contact perturbations. Before concluding, we present a discussion of these perturbations and the extent to which they may affect our experiments.

Voltage-sensing contacts on the surface of a sample shunt current out of the sample, modifying the electric field and CDW current distributions in their vicinity. As discussed by Maher *et al.*,[18] only the quasiparticle current density $j_n(x)$ is reduced beneath the contact if the amount of current shunting is sufficiently small. A CDW strain gradient develops in this region to offset the decrease in electric field and keep j_c constant, as illustrated in Fig. 11. If the voltage contact shunting is large, however, the strain $\epsilon(x)$ near the contact may become large enough to cause phase slip. This occurs more readily at the voltage contacts nearest the current contacts, where the macroscopic strain field is largest. In our experimental geometry, the measured CDW current profile is thus strongly perturbed if the change in strain caused by a voltage contact, $\Delta\epsilon_{pert}$, is comparable to the change in strain due to the macroscopic strain field between a current contact and the nearest voltage contact, $\Delta x(\partial\epsilon/\partial x)_{macro}$.

One way to test experimentally for phase slip induced by contact perturbations is to inject current through contacts 1 and 16 and measure the CDW current density profile $j_c^0(x)$ in the region between contacts 2 and 15. Since the current contacts are far away from this region, any phase slip observed can be attributed to voltage contact perturbations. As shown in Fig. 8, $j_c^0(x)$ is essentially constant at 90 K, indicating that

TABLE II. Comparison of the calculated strain difference caused by perturbations at a voltage electrode, $\kappa\Delta\epsilon_{\rm pert}$, with the strain difference $\Delta x\kappa(\partial\epsilon/\partial x)_{\rm macro}$ measured in sample 1 between adjacent contacts. $\kappa\Delta\epsilon_{\rm pert}$ is given for the cases of ideal nondissipative contacts (second column) and for a small contact interface resistance (third column). The contacts are perturbing when the magnitude of $\kappa\Delta\epsilon_{\rm pert}$ is comparable to or greater than that of $\Delta x\kappa(\partial\epsilon/\partial x)_{\rm macro}$. $\kappa\Delta\epsilon_{\rm macro}$ could not be measured at 135 K due to contact perturbations.

T (K)	$\kappa\Delta\epsilon_{\rm pert}$ (μV) (Ideal contacts)	$\kappa\Delta\epsilon_{\rm pert}$ (μV) (10 Ω μm2 contacts)	$\Delta x\kappa(\partial\epsilon/\partial x)_{\rm macro}$ (μV) ($\Delta x=20$ μm)
70	-5.2	-1.5	160 ± 1
90	-7.3	-2.1	63 ± 1
105	-8.5	-2.4	4 ± 1
120	-9.4	-2.7	2 ± 1
135	-9.1	-2.6	

contact perturbations are too small to cause phase slip in this geometry. Similar results were obtained for all experimental conditions presented here except at $T=135$ K, where $j_c^0(x)$ dipped due to phase slip near contacts (3,4) and (13,14). This dip was typically about half of that observed when injecting through pair (2,15), indicating that the triplets of contacts (2,3,4) and (13,14,15) were strongly perturbing at 135 K.[47]

This experimental test does not rule out phase slip due to contact perturbations below 135 K when injecting current at contacts 2 and 15, however, since in this case the voltage contacts are much closer to the current contacts where $\epsilon(x)_{\rm macro}$ is large. We estimate the importance of contact perturbations below 135 K using the model of Eq. (5). The magnitude of $\kappa\Delta\epsilon_{\rm pert}$ was evaluated by solving Laplace's equation numerically for the electric field distribution near a side voltage contact. Treating the contact as a perfect conductor with a perfect interface to the sample and assuming a sample thickness of 1.9 μm, an electrode width of 2 μm and a resistivity anisotropy $\rho_x/\rho_y=10$ yields that 14% of the quasiparticle current is shunted by the contact. A more realistic estimate including a finite interface resistance of 10 $\Omega\mu{\rm m}^2$ yields 4% shunting.[48]

The corresponding change in strain $\Delta\epsilon_{\rm pert}$ in the region under the contact due to perturbations is, from Eq. (5),

$$\Delta\epsilon_{\rm pert}=-(\rho_n/\kappa)\int[j_{\rm tot}^{\infty}-\langle j_{\rm tot}(x)\rangle]\,dx, \tag{10}$$

where $j_{\rm tot}^{\infty}$ is the current density far from the perturbing contact. From the numerical solution for the quasiparticle current distribution, we find $\kappa\Delta\epsilon_{\rm pert}=\alpha\rho_n j_{\rm tot}$, where $\alpha=0.20$ μm for ideal contacts and $\alpha=0.05$ μm for a finite contact resistance of 10 $\Omega\mu{\rm m}^2$.

Table II compares the calculated values of $\kappa\Delta\epsilon_{\rm pert}$ for a current density $j_{\rm tot}=3j_T(90\ {\rm K})=40.8\ \mu{\rm A}/\mu{\rm m}^2$ with the measured values of $\kappa\Delta\varepsilon_{\rm macro}\equiv\Delta x\kappa(\partial\epsilon/\partial x)_{\rm macro}$ in sample 1. The quoted values use $\Delta x=20$ μm, the shortest contact separation in our experiment, and $\kappa(\partial\epsilon/\partial x)_{\rm macro}$ measured in the center of the sample, where it has its smallest value. Note from the table that $\Delta x\kappa(\partial\epsilon/\partial x)_{\rm macro}$ decreases rapidly with increasing temperature while $\kappa\Delta\epsilon_{\rm pert}$ is relatively independent of temperature.

At 70 and 90 K, $\kappa\Delta\epsilon_{\rm pert}$ is much less than $\kappa\Delta\epsilon_{\rm macro}$ even in the very conservative case of ideal contacts, and we expect the voltage contacts to be essentially nonperturbing.

At 105 and 120 K, $\kappa\Delta\epsilon_{\rm pert}$ is comparable to $\kappa\Delta\epsilon_{\rm macro}$. Some phase slip is probably occurring near contacts 3, 4, 13, and 14 at 105 K. The effect is even more pronounced at 120 K, where we cannot rule out phase slip at any of the contacts.

At 135 K $\epsilon(x)$ could not be measured since, as discussed above, the contacts were completely perturbing. Extrapolating the trend of decreasing $\kappa\Delta\epsilon_{\rm pert}$ from lower temperatures using the $V_{\rm ps}$ measurements of Maher *et al.*[18] suggests that $\kappa\Delta\epsilon_{\rm pert}$ is roughly 200% of the strain necessary to cause phase slip at this temperature. This implies that the voltage contacts should be strongly perturbing, consistent with experiment.

V. CONCLUSIONS

We have measured the spatial distribution of CDW current density $j_c(x)$ and phase slip $r_{\rm ps}(x)$ for the T_{P_1} CDW of $NbSe_3$ using arrays of micron-scale contacts. We conclude from measurements and calculations that contact perturbations were negligible at temperatures well below the transition temperature. Appreciable phase slip occurs in regions that extend less than 40 μm from the current contacts at T near 120 K but grow to hundreds of micrometers at lower temperatures. The phase-slip profile is also asymmetric with respect to driving current direction, implying an asymmetry between phase front addition and removal.

Analysis of the CDW current profiles yields the CDW strain distribution $\epsilon(x)$ and the local $r_{\rm ps}$-ϵ relation. This relation is not unique: for a given strain, the phase-slip rate increases with distance from the current contacts. These observations are inconsistent with the predictions of models of phase slip via strain-driven homogeneous defect nucleation, and provide evidence for amplitude defect motion. The presence of substantial amounts of phase slip large distances from the current contacts explains the apparent loss of coherence of the sliding CDW at lower temperatures, and indicates that phase-only models of CDW dynamics may be largely inapplicable to the sliding CDW in $NbSe_3$. Our analysis of the strain profile measurements of Itkis *et al.* in $K_{0.3}MoO_3$ suggests that most of these conclusions also hold in that material.

ACKNOWLEDGMENTS

We wish to acknowledge fruitful discussions with S. V. Zaitsev-Zotov. Substrates were prepared at the Cornell Nanofabrication Facility. This work was supported by NSF Grant Nos. INT-9016655 and DMR94-24572. S.G.L. acknowledges additional support from NSERC.

APPENDIX: CORRECTIONS TO EQ. (4) FOR $r_{\rm ps}(x)$

From the definition of $r_{\rm ps}$, Eq. (1), we have

$$\langle j_c\rangle_{n+1,n}-\langle j_c\rangle_{n,n-1}=-\frac{en_c}{Q}\int_{x_{n-1}}^{x_{n+1}}r_{\rm ps}(x)\ g_n(x)\ dx, \tag{A1}$$

where

$$g_n(x)=\begin{cases}(x_{n+1}-x)/l_+, & x_n<x<x_{n+1}\\ (x-x_{n-1})/l_-, & x_{n-1}<x<x_n\\ 0, & \text{otherwise.}\end{cases} \tag{A2}$$

Here we defined $l_+=x_{n+1}-x_n$ and $l_-=x_n-x_{n-1}$. Equation (4) follows when the lengths l_+ and l_- are nearly equal and terms of second order and higher in a Taylor expansion of $r_{ps}(x)$ about x_n are small.

$r_{ps}(x)$ was found empirically to have the approximate form $r_{ps}(x)\approx r_{ps}^0 \exp(-x/a)$ away from the current contacts, where $x=0$ corresponds to such a contact. We use this expression to evaluate corrections to Eq. (4). Substituting into Eq. (A1), we find that the phase-slip rate calculated using the approximate Eq. (4) in fact corresponds to the phase-slip rate at

$$x=x_n-a\,\ln\frac{2a}{l_++l_-}\left[\frac{a}{l_-}\left(\exp\frac{l_-}{a}-1\right)+\frac{a}{l_+}\left(\exp\frac{-l_+}{a}-1\right)\right]. \tag{A3}$$

For a typical value of $a=80$ μm at 90 K, this indicates that the phase-slip rate for contacts 3 and 14 ($l_+=l_-=20$ μm) and contacts 5 through 12 ($l_+=l_-=70$ μm) as evaluated using Eq. (4) correspond to the phase-slip rate 0.4 μm and 5 μm from the contact toward the current electrode, respectively. These small corrections are on the same order as other systematic errors in the experiment. A larger correction is required for contacts 4 and 13 ($l_-=20$ μm, $l_+=70$ μm): because $l_+>l_-$, the measurement weights more heavily the l_+ segment. The phase-slip rate calculated from Eq. (4) corresponds to the phase-slip rate 19 μm from the contact toward the center of the sample. These corrections were applied to the data in Fig. 9 by extrapolating the strain linearly between adjacent contacts.

[1] For comprehensive reviews of CDWs, see P. Monceau in *Electronic Properties of Inorganic Quasi-One-Dimensional Compounds* (Reidel, Dordrecht, 1985), Pt. II, p. 139; G. Grüner, Rev. Mod. Phys. **60**, 1129 (1988); C. Schlenker *et al.*, in *Low-Dimensional Electronic Properties of Molybdenum Bronzes and Oxides*, edited by C. Schlenker (Kluwer, Dordrecht, 1989), p. 159.

[2] L. Sneddon, M. Cross, and D. Fisher, Phys. Rev. Lett. **49**, 292 (1982); H. Matsukawa and H. Takayama, J. Phys. Soc. Jpn. **56**, 1507 (1987); H. Matsukawa, *ibid.* **56**, 1522 (1987); **57**, 3463 (1988); S. N. Coppersmith and P. B. Littlewood, Phys. Rev. B **36**, 311 (1987).

[3] H. Fukuyama and P. A. Lee, Phys. Rev. B **17**, 535 (1978); P. A. Lee and T. M. Rice, *ibid.* **19**, 3970 (1979).

[4] D. S. Fisher, Phys. Rev. Lett. **50**, 1486 (1983); Phys. Rev. B **31**, 1396 (1985).

[5] A. A. Middleton and D. S. Fisher, Phys. Rev. B **47**, 3530 (1993).

[6] C. R. Myers and J. P. Sethna, Phys. Rev. B **47**, 11 171 (1993); **47**, 11 194 (1993).

[7] J. C. Gill, in *Physics and Chemistry of Low-Dimensional Inorganic Conductors*, edited by C. Schlenker and M. Greenblatt (Plenum, New York, 1996), p. 411–430.

[8] Y. Tanaka, M. I. Visscher, B. Rejaei, and G. E. W. Bauer, Physica B **227**, 339 (1996).

[9] K. Maki, Physica B **143**, 59 (1986).

[10] D. Feinberg and J. Friedel, in *Low-Dimensional Electronic Properties of Molybdenum Bronzes and Oxides*, edited by C. Schlenker (Kluwer, Dordrecht, 1989), p. 407.

[11] S. Ramakrishna, M. P. Maher, V. Ambegaokar, and U. Eckern, Phys. Rev. Lett. **68**, 2066 (1992); S. Ramakrishna, Phys. Rev. B **48**, 5025 (1993).

[12] M. Tinkham, *Introduction to Superconductivity*, 2nd ed. (McGraw-Hill, New York, 1996), p. 288.

[13] J. S. Langer and M. E. Fisher, Phys. Rev. Lett. **19**, 560 (1967).

[14] L. Mihály and A. Janossy, Phys. Rev. B **30**, 3530 (1984).

[15] S. E. Brown, L. Mihály, and G. Grüner, Solid State Commun. **58**, 231 (1986).

[16] J. C. Gill, Solid State Commun. **44**, 1041 (1982).

[17] D. V. Borodin, S. V. Zaitsev-Zotov, and F. Ya. Nad', Zh. Éksp. Teor. Fiz. **90**, 318 (1987) [Sov. Phys. JETP **66**, 793 (1987)].

[18] M. P. Maher, T. L. Adelman, S. Ramakrishna, J. P. McCarten, D. A. DiCarlo, and R. E. Thorne, Phys. Rev. Lett. **68**, 3084 (1992); M. P. Maher, T. L. Adelman, D. A. DiCarlo, J. P. McCarten, and R. E. Thorne, Phys. Rev. B **52**, 13 850 (1995).

[19] J. C. Gill, Phys. Rev. Lett. **70**, 331 (1993).

[20] M. E. Itkis and S. V. Zaitsev-Zotov, J. Phys. IV **3**, C2-193 (1993). Similar measurements were also carried out on TaS_3, but complications arise in this semiconducting material that were attributed to rectification at the junctions with the metal electrodes (Ref. 21).

[21] M. E. Itkis, F. Ya Nad', P. Monceau, and M. Renard, J. Phys.: Condens. Matter **5**, 4631 (1993).

[22] M. E. Itkis and J. W. Brill, Phys. Rev. Lett. **72**, 2049 (1994); M. E. Itkis, B. M. Emerling, and J. W. Brill, Phys. Rev. B **52**, R11 545 (1995).

[23] T. L. Adelman, M. C. de Lind van Wijngaarden, S. V. Zaitsev-Zotov, D. DiCarlo, and R. E. Thorne, Phys. Rev. B **52**, R5483 (1995); **53**, 1833 (1996).

[24] M. C. Saint-Lager, P. Monceau, and M. Renard, Europhys. Lett. **9**, 585 (1989;); Synth. Met. **29**, F279 (1989).

[25] Bulk Joule heating results in a maximum error of $\approx 0.5\%$ in j_c for the values of j_{tot} investigated. The CDW strain $\epsilon(x)$, which modifies the local quasiparticle resistance by $\delta\rho_n(x)/\rho_n = (n_c/n_{qp})\epsilon[x]\approx\epsilon(x)$, introduces a spurious asymmetry in $j_c(x)$ of a few % for near-threshold currents and 0.5–1% well above threshold [based on measured values of $\epsilon(x)<0.0025$ near a current contact at 90 K (Refs. 23 and 49)]. This asymmetry is opposite in sign to that observed here, so that the asymmetry in $j_c(x)$ reported in Secs. III A and III B is somewhat underestimated. Finally, fringing near the current contacts can also introduce error into the measured $j_c(x)$ since the electric-field distribution changes somewhat once the CDW depins. R_n for segments (9,5) and (11,8) is greater by $\approx 1\%$ when injecting current through pair (2,15) than when injecting through pair (1,16), yielding an error in j_c due to changes in the fringing pattern above threshold of the order of $0.01(j_c/j_{tot})\leqslant 0.25\%$. These sources of error are insufficient to affect the conclusions reached here.

[26] S. G. Lemay, R. E. Thorne, M. C. Saint-Lager, and P. Monceau, Phys. Rev. B **54**, 16 341 (1996).

[27] The temperature of 105 K selected for Fig. 7 is a compromise between clearly resolved mode-locking features and a pronounced curvature for $j_c(x)$.

[28] The r_{ps}-ϵ relation for the positive and negative contacts are nearly identical, except that the curves for the positive electrode are shifted toward higher r_{ps} by 10–20%. Averaging the two current directions yields an antisymmetric $\epsilon(x)$, removing the ambiguity in $\epsilon(x_0)$ in Eq. (7).

[29] More specifically, Maher *et al.*'s analysis of the four-probe measurements assumed that $V_{ps}=V_{strain}\equiv-\kappa\int_{in}(\partial\epsilon/\partial x)\,dx$ when in fact

$$V_{ps}=V_{strain}-\int_{out}[\rho_c+\rho_s]i_c^1(x)\,dx-\int_{in}[E_p(i_c^0)-E_p(i_c^1)]\,dx.$$

Here the integrals $\int_{in}$ and $\int_{out}$ are carried out over the region between and beyond the current contacts, respectively. The two correction terms are negative so that $V_{ps}<V_{strain}$, resulting in an overestimation of V_a when using this method.

[30] Adelman *et al.* (Ref. 23) estimated V_a = 31 mV at 90 K from preliminary high-current data obtained with contacts essentially identical to those used here. This value was probably overestimated due to Joule heating at the current contacts; fits to data for which such heating was present in our samples (not shown) also yield $V_a\approx$ 30 mV.

[31] The simulation uses $en_c/Q=4.33\times10^{-3}$ e Å^{-2}, $K=6.21\times10^{-3}$ eV Å^{-1}, $r_0=2\times10^{15}$ s^{-1} m^{-1}, $\rho_n=0.90$ Ω μm, and $\rho_c=3.69$ Ω μm at $T=90$ K, and $V_a=85$, 23, and 4.5 mV at $T=70$, 90, and 105 K, respectively. The experimentally determined $E_P(j_c)$ relation for sample 1 at each temperature is also used.

[32] M. P. Maher, T. L. Adelman, J. McCarten, D. A. DiCarlo, and R. E. Thorne, Phys. Rev. B **43**, 9968 (1991).

[33] S. N. Coppersmith and A. J. Millis, Phys. Rev. B **44**, 7799 (1991).

[34] M. E. Itkis, B. M. Emerling, and J. W. Brill, Synth. Met. **86**, 1959 (1997).

[35] J. C. Gill, Europhys. Lett. **11**, 175 (1990).

[36] The time-dependent form of Eqs. (5)–(6) reduces to the model used by Gill to describe nonuniform current-injection conditions (Ref. 35) upon linearizing about the steady-state solution. The drift velocity constant V in Ref. 35 correponds to $-\beta/en_c(\rho_n+\rho_c)$ in the notation used here.

[37] The procedure is a straightforward extension of that used in Sec. IV A. Instead of Eq. (7), $\epsilon(x)$ is now given by the solution to

$$\frac{\partial\epsilon}{\partial x}+(\beta/\kappa)\epsilon=\frac{\rho_c+\rho_n}{\kappa}\left[j_c^1-j_c^0+\frac{E_P(j_c^1)-E_P(j_c^0)}{\rho_c+\rho_n}\right]. \quad \text{(A4)}$$

All quantities on the right-hand side are directly measurable, but the parameter β/κ must be determined separately.

[38] Assuming parabolic bands.

[39] R. E. Thorne, Ph.D. thesis, University of Illinois at Urbana-Champaign, 1987.

[40] P. Monceau, J. Richard, and M. Renard, Phys. Rev. B **25**, 931 (1982).

[41] J. Richard, J. Chen, and S. N. Artemenko, Solid State Commun. **85**, 605 (1993).

[42] J. McCarten, D. A. DiCarlo, M. P. Maher, T. L. Adelman, and R. E. Thorne, Phys. Rev. B **46**, 4456 (1992).

[43] M. O. Robbins, J. P. Stokes, and S. Bhattacharya, Phys. Rev. Lett. **55**, 2822 (1985); W. Xue-mei, Z. Dian-lin, and Z. Yuheng, Phys. Rev. B **45**, 13 250 (1992).

[44] M. J. Higgins, A. A. Middleton, and S. Bhattacharya, Phys. Rev. Lett. **70**, 3784 (1993).

[45] S. N. Coppersmith, Phys. Rev. Lett. **65**, 1044 (1990).

[46] In $K_{0.3}MoO_3$, the modulation of the quasiparticle resistivity ρ_n by the CDW strain ϵ is more pronounced than in $NbSe_3$. Since the experimentally observed profiles are nearly symmetric, however, it is reasonable to ignore this correction in the first approximation.

[47] Similar perturbations were also observed below 135 K in some samples when using thick (0.3 μm) chromium electrodes. These anomalies are believed to result from local strains in the crystal lattice where the $NbSe_3$ whisker deforms around the electrode. This is supported by the near absence of such anomalies when using thinner (0.1 μm) electrodes.

[48] Each photolithographically patterned Au-Cr wire has a room-temperature resistance of about 220 Ω, making it difficult to measure the impedance of the Au-$NbSe_3$ interfaces directly. The interface resistance of 10 Ω μm^2 was estimated from data on Maher's (Ref. 18) indium contacts; the value for the Au-Cr wires is expected to be somewhat higher, making this a conservative estimate.

[49] D. DiCarlo, E. Sweetland, M. Sutton, J. D. Brock, and R. E. Thorne, Phys. Rev. Lett. **70**, 845 (1993).